Water Science & Technology

Water Science & Technology Vol 00 No 0, 1 doi: 10.2166/wst.2026.288

Boosting photocatalytic mineralization of polystyrene microplastics with a TiO_2@UiO-66 advanced semiconductor composite

Xuan N. Pham [a,*], Huan V. Doan [a,b] and T.-Thanh-Bao Nguyen [c]

[a] Department of Chemical Engineering, Hanoi University of Mining and Geology, 18 Pho Vien, Duc Thang, Bac Tu Liem, Hanoi, Vietnam
[b] Research School of Chemistry, The Australian National University, Canberra, ACT 2601, Australia
[c] Institute of Physics, Vietnam Academy of Science and Technology, 18C Hoang Quoc Viet, Hanoi, Vietnam
*Corresonding author. E-mail: phamxuannui@humg.edu.vn

NPX, 0000-0002-7469-3001; HVD, 0000-0002-8757-364X; T-T-BN, 0000-0001-6802-9481

ABSTRACT

Photocatalysis is a promising technology for the removal of microplastics from aquatic environments. A current research focus lies in developing photocatalytic materials capable of efficiently degrading microplastics under visible or ultraviolet (UV) light irradiation. In this study, a TiO_2@UiO-66 heterostructured nanocomposite was synthesized and employed for the photocatalytic degradation of polystyrene (PS) microplastics under UV illumination at room temperature. The synthesized materials were characterized by XRD, SEM, UV–Vis/DRS, PL spectroscopy, XPS, and EDX mapping. The TiO_2@UiO-66 composite exhibited significantly higher photocatalytic activity toward PS microplastic degradation compared with pristine TiO_2 and UiO-66 under UV light irradiation. Approximately 63% of PS microplastics (150 ppm) were degraded after 30 h of irradiation at an intensity of 4 mW·cm^{-2} under natural pH conditions. The analysis of total organic carbon indicated a decline in the removal efficiency of PS microplastics with increasing concentration. Liquid chromatography–mass spectrometry and Fourier transform infrared analyses revealed the formation of soluble organic intermediates such as aldehydes and carboxylic acids during the degradation process. These results demonstrate that the TiO_2@UiO-66 photocatalyst is a promising material for the removal of PS microplastics in aqueous environments, where the $^{\bullet}OH$, $O_2^{\bullet -}$ play a dominant role in the degradation mechanism.

Key words: degradation, photocatalyst, polystyrene microplastics, TiO_2@UiO-66, UV

HIGHLIGHTS

- The TiO_2@UiO-66 composite photocatalyst was synthesized through a simple hydrothermal process using waste PET as a precursor.
- The reactive radical species (•OH) and ($\bullet O_2^-$) played a dominant role in the photocatalytic degradation of polystyrene microplastics.
- Intermediate products, including aldehydes and carboxylic acids, were formed during the photocatalytic degradation of PSMPs.

GRAPHICAL ABSTRACT

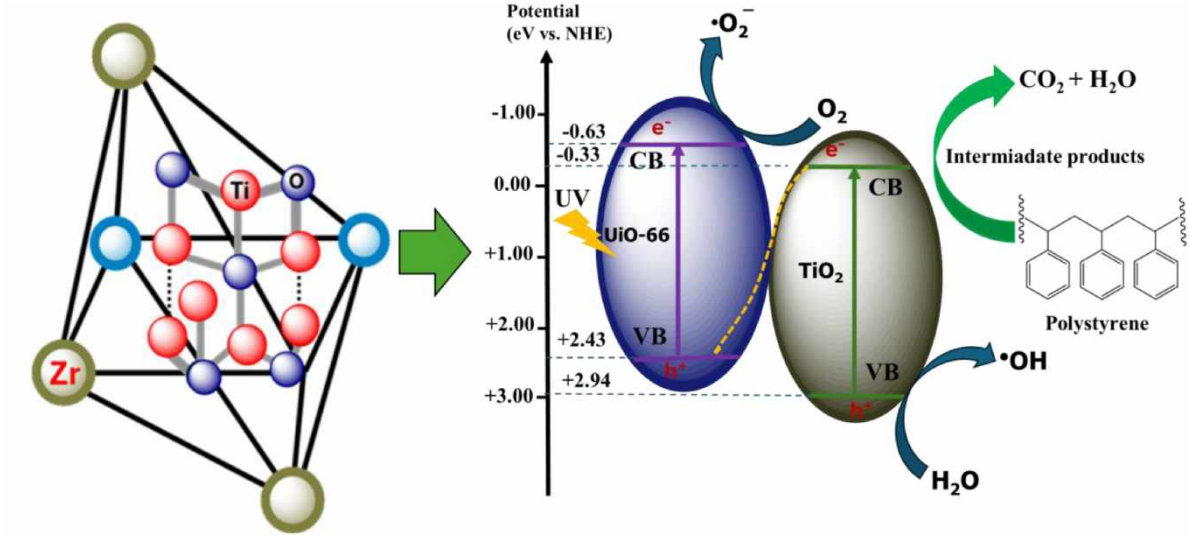

1. INTRODUCTION

Currently, more than 300 million tons of plastics are produced annually, and it is estimated that approximately 13 million tons are discharged into rivers and oceans each year (Li *et al.* 2024). Microplastics (MPs) are generated through the fragmentation of larger plastic debris as a result of physical, chemical, and biological processes in the environment (Galgani *et al.* 2013; Law 2017; González-Pleiter *et al.* 2019). These particles infiltrate marine and freshwater systems, becoming a major environmental concern. Microplastics are now recognized as contaminants of emerging concern (CECs) due to their adverse impacts on ecosystems and human health, primarily through the alteration of ecosystem quality and disruption of food chains (Schirinzi *et al.* 2017; Kögel *et al.* 2020). However, research on strategies for mitigating, remediating, or removing microplastics from aquatic environments remains in its infancy and has only gained significant attention within the past five years (Karimi Estahbanati *et al.* 2021).

Several physicochemical methods have been investigated for the removal of microplastics from water. For instance, coagulation/flocculation and electrocoagulation processes have been employed; however, they often generate large quantities of sludge containing high plastic content (Padervand *et al.* 2020). In addition, biological approaches, such as membrane bioreactor systems, rely heavily on the type of microorganisms and soil conditions, requiring strict operational and maintenance conditions (Amjad *et al.* 2023). Following the development of advanced oxidation processes (AOPs), which are considered highly promising technologies for the degradation of dissolved pollutants in water, their application to the complete removal of microplastics has emerged as a new and rapidly growing research field. Among these approaches, photocatalytic degradation of polymers using semiconductor photocatalysts has been identified as one of the most promising methods. These photocatalysts can efficiently harness light energy from mercury lamps, ultraviolet irradiation, halogen lamps, visible light, and solar radiation to degrade polymeric materials. Notably, solar light is an abundant and sustainable energy source that contains approximately 3–5% UV, 47% visible, and infrared radiation (Bora & Mewada 2017).

According to the photocatalytic mechanism, the catalyst absorbs photon energy and generates photo-induced electron–hole pairs, which subsequently produce various reactive oxygen species (ROS) such as superoxide radicals ($O_2^{\bullet -}$), hydroxyl radicals ($^{\bullet}OH$), and hydroperoxyl radicals ($^{\bullet}OOH$). These ROS species interact with surrounding media, thereby initiating and accelerating oxidative degradation of polymer chains (Tofa *et al.* 2019a, 2019b). A wide range of nanostructured photocatalysts – including titanium dioxide (TiO_2), zinc oxide (ZnO), tin oxide (SnO_2), iron oxides (Fe_2O_3/Fe_3O_4), and tungsten oxide (WO_3)—have been widely investigated due to their strong light sensitivity in both the UV and visible regions (Tofa *et al.* 2019a, 2019b). Among them, TiO_2 nanoparticles are particularly noteworthy for their ability to absorb a broad portion of the solar spectrum, including visible light, making them one of the most effective photocatalysts for environmental remediation (Jianhua *et al.* 2022; Danilo & Ana 2025; Xueqin *et al.* 2025).

Pioneering studies have been conducted on the heterogeneous photocatalytic degradation and mineralization of microplastics such as high-density polyethylene (HDPE) and low-density polyethylene (LDPE) in aqueous environments.

Specifically, a green C,N-doped TiO_2 photocatalyst immobilized on cellulose nanofibers (CNF) has been investigated for the removal of polyethylene (PE) microplastics (Ariza-Tarazona *et al.* 2019). Similarly, ZnO nanoparticles under natural sunlight have been reported to effectively reduce polyethylene microplastics in wastewater (Raji & Gopchandran 2019; Jeyaraj & Baskaralingam 2023; Montenegro *et al.* 2025). In addition, the photocatalytic degradation of polystyrene and poly(methyl methacrylate) (PMMA) nanoparticles has been achieved using TiO_2–P25/β-SiC foam composites under UV-A irradiation (Allé *et al.* 2021; Domínguez-Jaimes *et al.* 2021). Moreover, the degradation of nylon-6 microfibers was demonstrated using a (Cu/Fe)-derived CuO/TiO_2 photocatalyst (Rodríguez-Olivares *et al.* 2025), while polyethylene terephthalate (PET) nanoplastics were effectively decomposed by a TiO_2/MIL-100(Fe) composite photocatalyst (Rojas-Guerrero *et al.* 2023). Recently, a green semiconductor-based N–TiO_2 mesoporous photocatalyst derived from protein achieved a 6.4% mass reduction of HDPE microplastics after 18 h of visible-light irradiation (Ariza-Tarazona *et al.* 2019). Similarly, solid-phase photocatalytic degradation of polystyrene using TiO_2 photocatalysts under UV radiation in air has been reported (Shang *et al.* 2003), and $TiO_2/Fe(St)_3$ composites demonstrated a mass loss of up to 79.49% for composite films after 480 h of UV exposure (Fa *et al.* 2012). However, TiO_2 can only be activated by UV light due to its wide band gap (E_g = 3.2 eV), which significantly limits its photocatalytic performance under visible-light conditions (Ariza-Tarazona *et al.* 2020). In contrast, metal–organic frameworks (MOFs)—well known for their highly porous structures and large specific surface areas (100–2,000 $m^2 \cdot g^{-1}$)—offer new opportunities for improving photocatalytic activity. The integration of TiO_2 with MOFs can introduce metal coordination centers that enhance light absorption, promote photoinduced charge separation, or serve as electron-trapping sites within the semiconductor matrix, thereby improving overall photocatalytic efficiency.

In this study, the TiO_2@UiO-66 composite photocatalyst was synthesized for the removal of microplastics from wastewater. The obtained photocatalyst was characterized using various physicochemical techniques, and its photocatalytic performance toward the degradation of polystyrene microplastics under UV irradiation in aqueous media. Furthermore, analytical techniques including FT-IR, UV–Vis spectroscopy, and LC/MS were employed to investigate the degradation mechanism and transformation pathways of polystyrene microplastics.

2. EXPERIMENTAL

2.1. Materials

Terephthalic acid (99.5%) was recovered from waste PET (Doan *et al.* 2021); titanium(IV) isopropoxide (TTIP, 97%, Sigma-Aldrich); glacial acetic acid (99%, Sigma-Aldrich); ethanol (99.5%, Acros); zirconium(IV) chloride (99.5%); N,N-dimethylformamide (DMF, 99.8%, Sigma-Aldrich); hydrochloric acid (HCl, 37%, Sigma-Aldrich); and polystyrene microplastic suspension (5% w/v in water, Sigma-Aldrich) were used as received without further purification.

2.2. Synthesis of TiO_2@UiO-66 composite photocatalyst

2.2.1. Synthesis of UiO-66

To synthesize UiO-66, $ZrOCl_2 \cdot 8H_2O$ (1.05 g, 3.16 mmol) was dissolved in a mixture of glacial acetic acid (4 mL) and DMF (45 mL) under ultrasonic treatment to obtain a clear solution. Subsequently, terephthalic acid (0.997 g, 6 mmol) was dispersed in DMF (20 mL) and added to the above solution. The mixture was stirred for 24 h at room temperature, then transferred into a Teflon-lined stainless-steel autoclave and heated at 120 °C for 36 h. The resulting solid was collected by centrifugation, washed several times with DMF and ethanol at 70 °C, and dried under vacuum at 120 °C overnight.

2.2.2. Synthesis of TiO_2

Titanium dioxide (TiO_2) was synthesized via the sol–gel method. In a typical procedure, TTIP (20 mL) was dissolved in ethanol (32 mL) under continuous stirring to form a homogeneous solution. A second solution containing distilled water (8 mL), ethanol (32 mL), and glacial acetic acid (16 mL), corresponding to a molar ratio of $H_2O : C_2H_5OH : CH_3COOH = 1 : 4 : 2$, was slowly added dropwise to the TTIP solution under constant stirring. The resulting mixture was stirred for 24 h at room temperature to form a gel, which was then dried at 100 °C for 12 h to obtain TiO_2 powder.

2.2.3. Synthesis of TiO_2@UiO-66

To synthesize the TiO_2@UiO-66 composite, 500 mg of UiO-66 was suspended in 50 mL of ethanol, followed by the addition of 10 mL of titanium(IV) isopropoxide under stirring for 1 h. Subsequently, a mixture of 25 mL ethanol and 10 mL HCl was added dropwise, and the suspension was stirred for an additional 3 h at room temperature. The mixture was then transferred

into an autoclave and heated at 120 °C for 24 h. The obtained solid was collected by centrifugation, dried at 100 °C overnight, and calcined in air at 350 °C for 2 h to yield the TiO_2@UiO-66 composite material.

2.3. Photocatalytic degradation of polystyrene microplastics

Batch photocatalytic degradation experiments were conducted under atmospheric pressure at room temperature (30 °C) and natural pH. Reactions were carried out in a 50 mL suspension containing a defined concentration of PS microplastics and 50 mg of photocatalyst under continuous stirring (600 rpm). Prior to irradiation, the mixture was stirred in the dark for 30 min to achieve adsorption–desorption equilibrium. The suspension was then irradiated with a 30 W UV lamp (λ = 365 nm) positioned at a distance of 10 cm, corresponding to an intensity of approximately 4 mW × cm^{-2}.

After illumination, samples were centrifuged to separate the catalyst powder from the aqueous phase. The supernatant was analyzed by UV–Vis spectroscopy at λ_{max} = 261 nm, while the dried photocatalyst was characterized by FT–IR and SEM after drying at 100 °C. The total organic carbon content of the filtrate (filtered through a 0.45 μm Phenex RC syringe filter) was measured using a TOC analyzer (TOC-VCSH, Shimadzu, Japan). The intermediate degradation products of polystyrene were identified using liquid chromatography–mass spectrometry (LC/MS, Waters XEVO TQ-XS).

Radical-trapping experiments were conducted to identify the reactive species involved in the photocatalytic degradation of PSMPs. In each batch experiment, 50 mg of TiO_2@UiO-66 was added to 50 mL of a PSMPs suspension (150 ppm). Subsequently, tert-butyl alcohol (TBA, 5 mM), *p*-benzoquinone (BQ, 5 mM), and formic acid (FA, 5 mM) were introduced as scavengers to selectively quench hydroxyl radicals ($^{\cdot}OH$), superoxide radicals ($O_2^{\bullet-}$), and photogenerated holes (h^+), respectively.

2.4. Characterization

X-ray diffraction (XRD) patterns were obtained using a Bruker D8 Advance diffractometer with Cu Kα radiation (λ = 0.15406 nm) in the 2θ range of 5–50°. Elemental composition and distribution were analyzed using energy-dispersive X-ray spectroscopy and mapping (JEOL JED-2300). Surface morphology was examined by scanning electron microscopy (SEM, HITACHI S-4800-3000F). Fourier-transform infrared spectra were recorded on a Jasco FT/IR-4700 spectrometer using KBr pellets. UV–Vis diffuse reflectance (UV-2600, Shimadzu) and photoluminescence (PL, Cary Eclipse) spectra were used to evaluate optical properties. X-ray photoelectron spectroscopy (XPS) measurements were carried out on a Thermo VG Multilab 2000 system to analyze surface elemental states.

3. RESULTS AND DISCUSSION

3.1. Structural characterization of the materials

Figure 1(a) shows the XRD pattern of UiO-66, confirming the successful formation of its crystalline framework. The characteristic diffraction peaks observed at 2θ = 7.4°, 8.4°, 17.13°, 25.57°, and 30.76° correspond to the (111), (200), (400), (442), and (440) crystal planes, respectively. These peaks are consistent with previously reported data for UiO-66

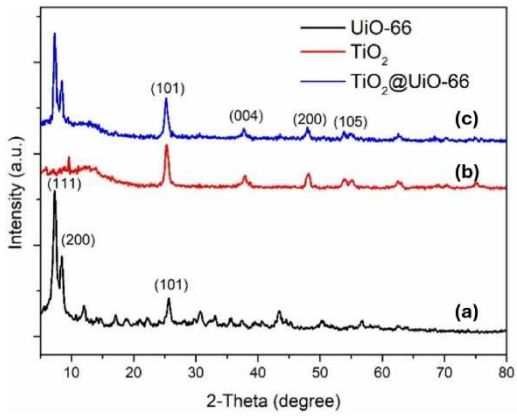

Figure 1 | XRD patterns of UiO-66 (a), TiO_2 (b), and TiO_2@UiO-66 composite (c).

(Viana *et al.* 2019) and match well with the standard reference pattern. The diffraction peaks of UiO-66 exhibit high intensity and sharpness, particularly the main peak at $2\theta = 7.4°$, indicating the high crystallinity and well-defined structure of the synthesized material.

Figure1(b) presents the XRD pattern of TiO_2 nanoparticles, showing distinct peaks characteristic of the anatase phase at $2\theta = 25.32°$, 37.92°, 48.08°, 54.02°, 62.62°, 68.93°, and 75.22°, which correspond to the (101), (004), (200), (105), (204), (116), and (215) planes, respectively. These results are in good agreement with previously reported TiO_2 patterns (Ramasubbu *et al.* 2022). The strong and sharp diffraction peaks, especially the dominant one at $2\theta = 25.32°$, indicate that the TiO_2 nanoparticles possess high crystallinity and a well-developed anatase phase structure. The XRD pattern of the TiO_2@UiO-66 composite displays the characteristic peaks of both UiO-66 and TiO_2, with distinct reflections at $2\theta = 7.4°$, 8.4°, 25.32°, 37.92°, and 48.08°, corresponding to the (111), (200), (101), (004), and (200) planes, respectively. The coexistence of these peaks confirms the successful integration of TiO_2 nanoparticles onto the UiO-66 framework without altering their crystalline structures. Based on the Debye–Scherrer equation, the estimated crystallite sizes of UiO-66, TiO_2, and TiO_2@UiO-66 were 6.8, 4.38, and 9.3 nm, respectively, indicating that the formation of the composite slightly increased the average crystallite size due to the incorporation and intergrowth of TiO_2 nanoparticles within the UiO-66 matrix.

The surface morphology of UiO-66, TiO_2, and TiO_2@UiO-66 was characterized using scanning electron microscopy, as shown in Figure 2. Figure 2(a) reveals that UiO-66 exhibits a relatively uniform octahedral crystalline structure with smooth surfaces, typical of well-crystallized UiO-66 frameworks. Figure 2(b) shows that TiO_2 nanoparticles possess a spherical morphology with a homogeneous particle distribution. In Figure 2(c), the TiO_2@UiO-66 composite displays well-dispersed TiO_2 nanoparticles distributed uniformly over the surface of UiO-66, confirming the successful immobilization of TiO_2 on the MOF framework without significant aggregation.

The optical properties of photocatalysts play a crucial role in determining their photocatalytic performance. Therefore, diffuse reflectance UV–Vis spectroscopy was employed to investigate the optical characteristics of UiO-66, TiO_2, and TiO_2@UiO-66, as illustrated in Figure 3(a).

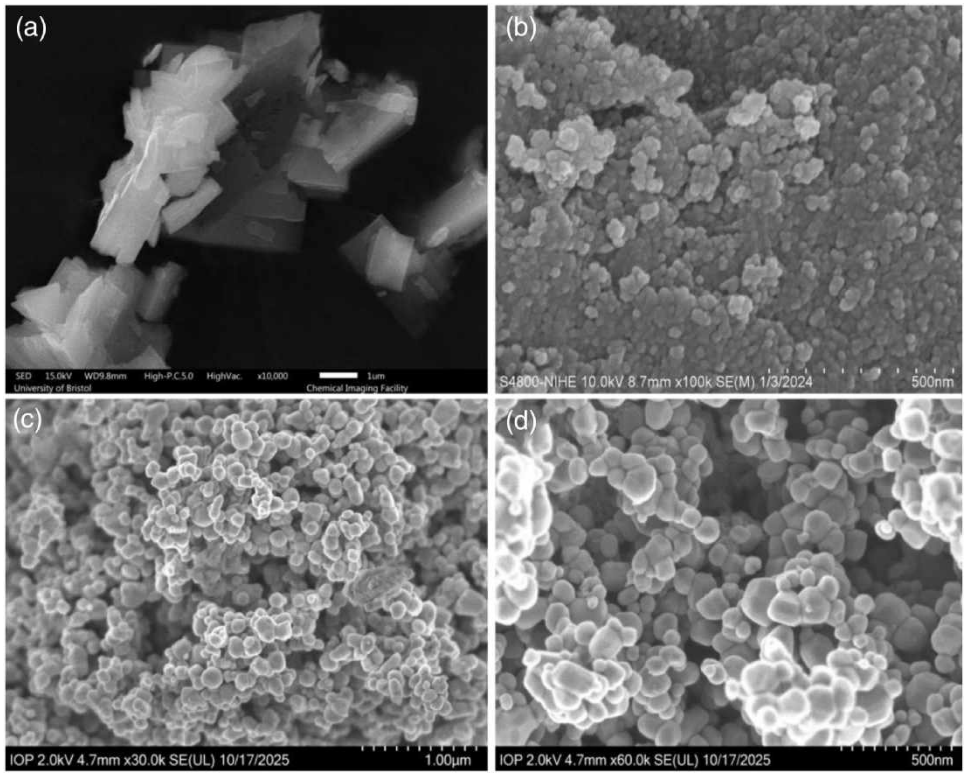

Figure 2 | SEM images of UiO-66 (a), TiO_2 (b), and TiO_2@UiO-66 composite (c) and (d).

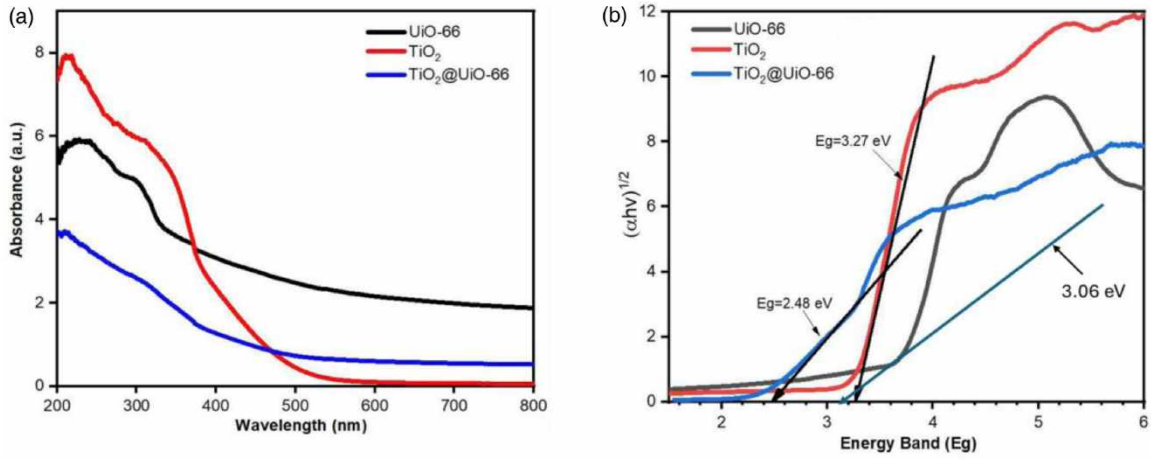

Figure 3 | UV–Vis absorption spectra (a), and Tauc plots for determining the band gap energy (E_g) (b) of TiO_2, UiO-66, and TiO_2@UiO-66 composite.

As shown in Figure 3(a), the TiO_2@UiO-66 composite exhibits a significantly enhanced light absorption ability within the visible region. Furthermore, the band gap energy (E_g) of the materials can be estimated using the Tauc equation:

$$\alpha h\nu = A(h\nu - E_g)^{n/2} \tag{1}$$

where E_g is the band gap energy of the semiconductor, A is the absorption constant, h is Planck's constant, α is the absorption coefficient, and ν is the light frequency. The value of n equals 1 for direct band gap semiconductors and 4 for indirect ones. The plots of ($\alpha h\nu$) versus photon energy ($h\nu$) shown in Figure 3(b) yield the estimated band gap energies of 3.06 eV, 3.27, and 2.48 eV for UiO-66, TiO_2, and TiO_2@UiO-66, respectively. The lower band gap value of the TiO_2@UiO-66 composite compared with pristine TiO_2 and UiO-66 indicates the formation of a heterojunction structure between TiO_2 and UiO-66. This structure facilitates the excitation of electrons and the generation of photogenerated electron–hole pairs under light irradiation, thereby significantly enhancing the photocatalytic activity (Cao *et al.* 2023).

Moreover, the photoluminescence spectrum of TiO_2@UiO-66 displays a lower emission intensity than that of pure TiO_2 and UiO-66 (Figure 4). This phenomenon may result from the formation of a Schottky barrier at the TiO_2/UiO-66 interface, which can serve as an electron reservoir within the defect structure of the composite. This behavior, confirmed by XPS results, suggests more efficient separation of photogenerated charge carriers (Chen *et al.* 2007; Lim *et al.* 2011;

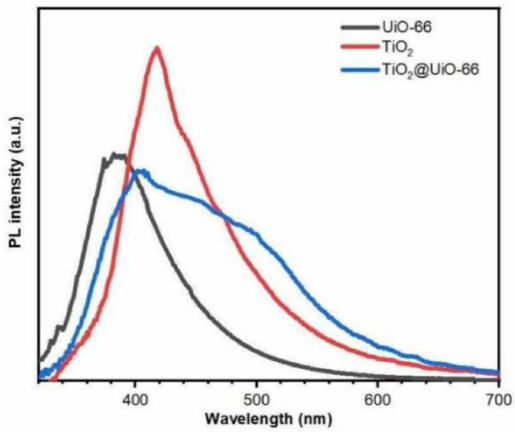

Figure 4 | Photoluminescence spectra of TiO_2, UiO-66, and TiO_2@UiO-66 composite materials.

Pham *et al.* 2022). A similar enhancement of electron–hole separation has been reported in the $CuInS_2$//MIL-101(Cr) system, which was attributed to interfacial electron transfer across the $CuInS_2 \rightarrow$ MIL-101(Cr) nanoscale junction (Nguyen *et al.* 2023).

The surface morphology and microstructure of the synthesized materials are illustrated in Figure 5. The EDX elemental mapping of TiO_2@UiO-66 confirms the presence of Ti, Zr, O, and C elements within the composite, further verifying the successful synthesis of the TiO_2@UiO-66 heterostructure.

As shown in Figure 6(a), the surface chemical composition and oxidation states of the elements in TiO_2@UiO-66 were further investigated using XPS. The XPS survey spectrum confirms that the composite is mainly composed of Ti, Zr, C, and O elements, which is consistent with the EDX results and the expected composition of the TiO_2@UiO-66 material.

Figure 6(b) shows the high-resolution Ti 2p spectrum, where three peaks corresponding to Ti^{4+} and Ti^{3+} species can be observed. The characteristic peaks of Ti^{4+} $2p_{1/2}$ and Ti^{4+} $2p_{3/2}$ appear at 464.3 and 458.6 eV, respectively, which are in good agreement with previous reports (Talal *et al.* 2024). The additional peak at 457.1 eV is assigned to Ti^{3+} $2p_{3/2}$, indicating

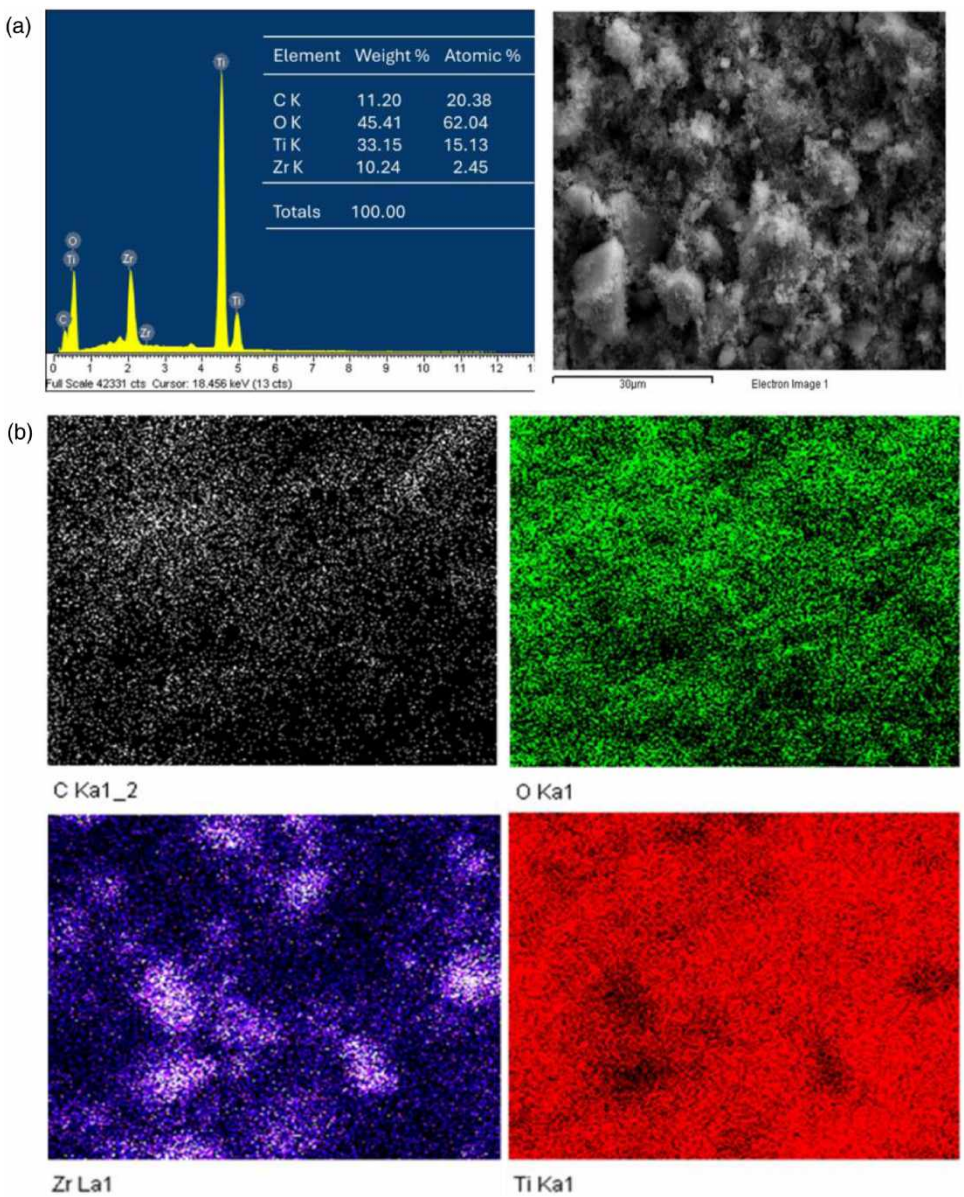

Figure 5 | EDX spectrum (a), and individual elemental mapping images of the TiO_2@UiO-66 composite (b).

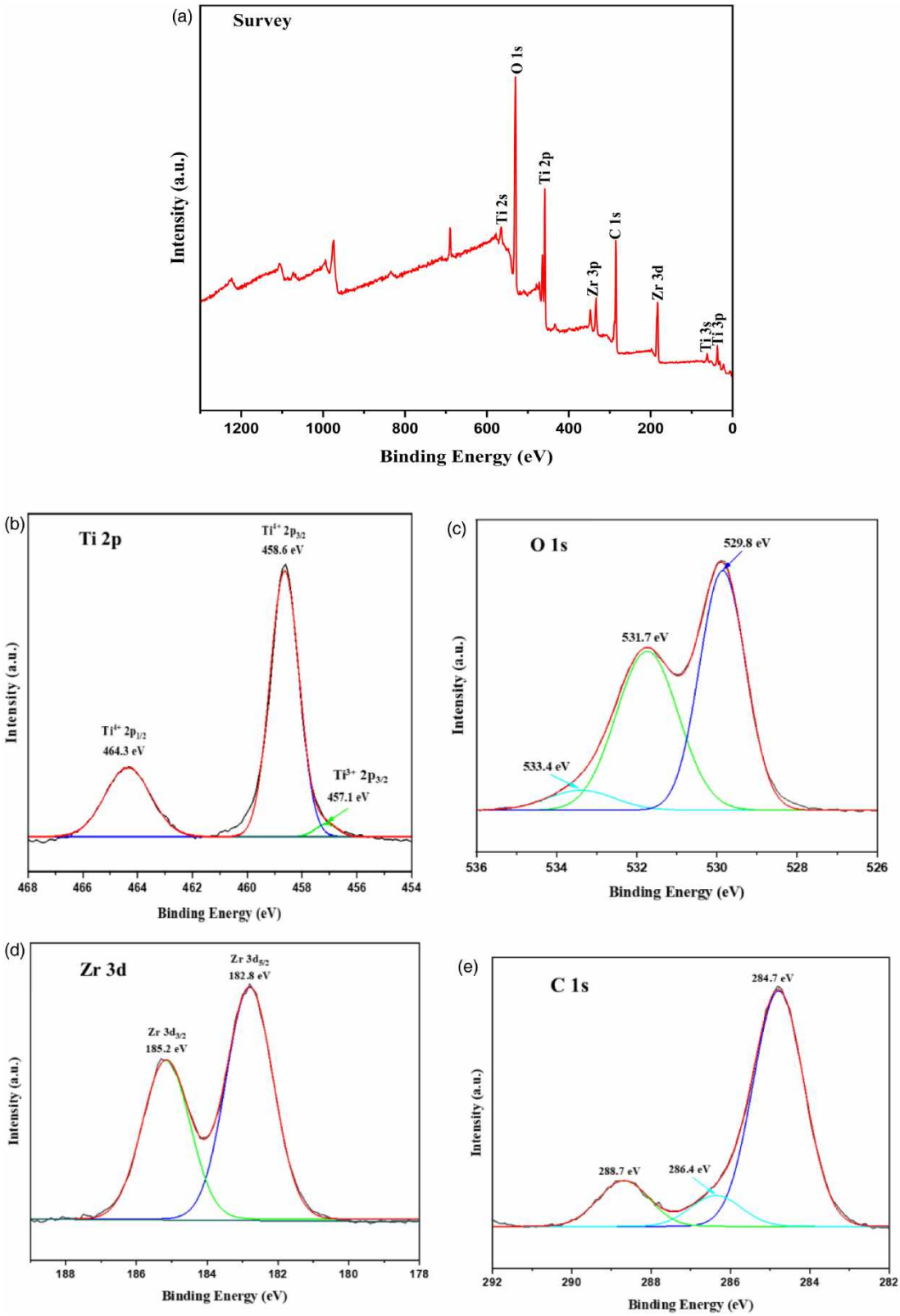

Figure 6 | XPS survey spectrum of TiO_2@UiO-66 (a), Ti 2p (b), O 1 s (c), Zr 3d (d), and C 1 s spectra (e).

the partial reduction of Ti^{4+} to Ti^{3+}, which results in the formation of oxygen vacancies within the composite semiconductor (Petri *et al.* 2020; Qahtan *et al.* 2024).

In the O 1 s spectrum (Figure 6(c)), the peaks located at 529.8, 531.7, and 533.4 eV correspond to Zr–O, Ti–O/C = O, and O–H groups, respectively. Meanwhile, the two peaks at 182.8 and 185.2 eV in Figure 6(d) are attributed to Zr $3d_5/_2$ and Zr $3d_3/_2$, confirming the presence of zirconium in UiO-66. The C 1 s spectrum of TiO_2@UiO-66 (Figure 6(e)) exhibits three peaks at 284.7, 286.4, and 288.7 eV, which are assigned to C–C, C–O, and O–C = O/C = O bonds, respectively (Valenzano *et al.* 2011; Cao *et al.* 2023). These results further confirm the successful synthesis of the TiO_2@UiO-66 composite material.

3.2. Photocatalytic degradation of polystyrene microplastics

In this study, the photocatalytic activity of the as-prepared catalysts was evaluated through the degradation of PSMPs under UV irradiation. As shown in Figure 7(a), the concentration of PSMPs shows only a slight decrease under UV illumination alone, with a degradation efficiency of about 4% after 30 h, confirming that photolysis has a negligible effect. Among all catalysts, TiO_2@UiO-66 exhibited the highest photocatalytic efficiency, achieving 63.4% degradation of PSMPs after 30 h of irradiation, including approximately 18.3% attributed to dark adsorption. In comparison, UiO-66 alone showed an adsorption efficiency of 16.2% in the dark, which was higher than that of pure TiO_2—likely due to the large specific surface area and high porosity of the MOF structure (Xu *et al.* 2021).

The increased surface area enhances the adsorption capability of TiO_2@UiO-66, while the aromatic structure of PSMPs facilitates π–π interactions with the benzene rings in UiO-66, leading to stronger adsorption (Alisha *et al.* 2025). Furthermore, the organic ligand (terephthalic acid) in UiO-66 can absorb visible light and transfer electrons to TiO_2, enabling visible-light photocatalytic activity. The Z-scheme charge transfer mechanism between UiO-66 and TiO_2 allows the recombination of low-energy electrons in TiO_2 with holes in UiO-66, preserving high-energy electrons and strong oxidative holes, thus enhancing the redox ability and improving PSMPs degradation efficiency.

As shown in Figure 7(b), photocatalytic degradation was conducted using 50 mg of TiO_2@UiO-66 for 50 mL of PSMPs solution at different concentrations under 30 h of continuous UV irradiation. The TOC removal reached 87.22 mg/L for 150 ppm PSMPs (initial TOC = 138 mg/L), which was higher than that obtained at higher concentrations of 200 ppm (78.40 mg/L) and 300 ppm (66.04 mg/L). This trend can be due to the reduced light penetration and limited contact between PS particles and the catalyst surface at higher concentrations. The dense suspension of PSMPs hinders light transmission and blocks the catalyst surface, reducing the generation of photoinduced electron–hole (e^-–h^+) pairs. Additionally, the deposition of PS layers or polymeric films on the catalyst surface can further lower the number of active sites and restrict the formation of reactive oxygen species ($^{\cdot}OH$, $\cdot O_2^-$), resulting in slower oxidation and reduced photocatalytic efficiency.

This study investigates the influence of catalyst dosage TiO_2@UiO-66 on photocatalytic performance. As shown in Figure 8(a), increasing the catalyst amount enhances the removal efficiency of microplastics during the dark adsorption

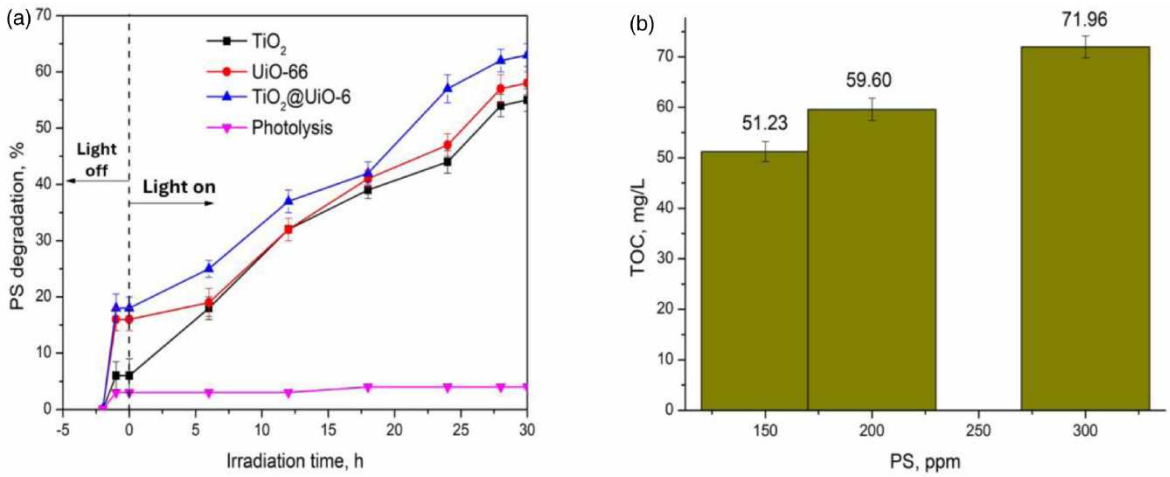

Figure 7 | Control experiments: Photocatalytic degradation efficiency of PS microplastics (150 ppm) using TiO_2, UiO-66, and TiO_2@UiO-66 catalysts (a); residual TOC content in the solution after photocatalytic degradation of PS microplastics at different initial concentrations using TiO_2@UiO-66 composite (b). (Conditions: 1.0 g/L of catalyst; natural pH, room temperature, light intensity = 4 mW·cm^{-2}).

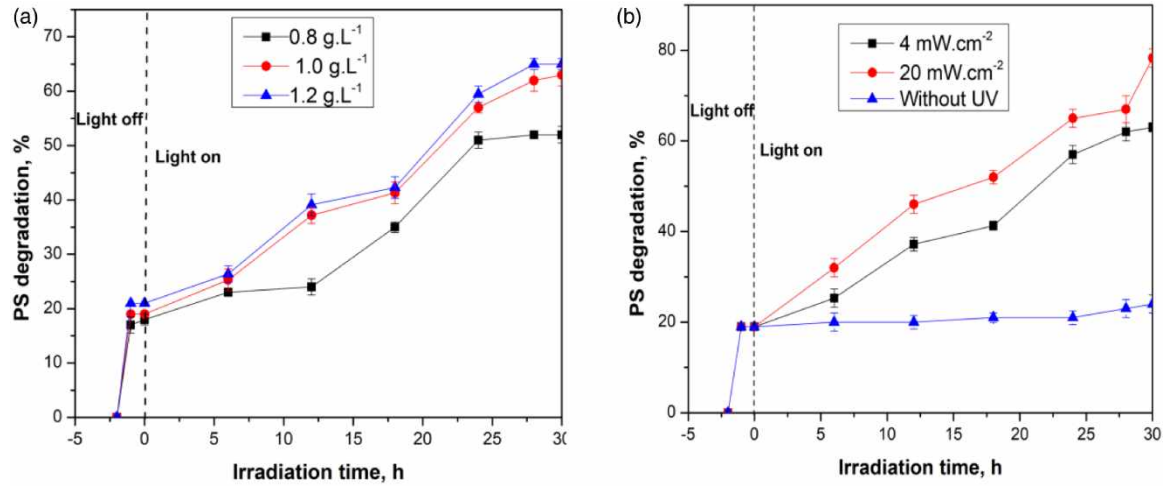

Figure 8 | (a) Effect of catalysts dosage TiO_2@UiO-66 on photocatalytic degradation of PSMPs under 4 mW·cm^{-2} of light intensity); and (b) light intensity on the removal of PSMPs with 1.0 g·L^{-1} TiO_2@UiO-66 photocatalyst. (Conditions: PSMPs = 150 ppm; natural pH, room temperature).

stage. However, during the photocatalytic reaction period (0–30 h), the degradation rate at a dosage of 1.2 g·L^{-1} increases only slightly compared to 1.0 g·L^{-1}, and subsequently the reaction rate slows and reaches a plateau. This behavior is likely attributed to the higher catalyst loading hindering light penetration into the suspension or reducing the amount of effectively accessible surface area (Wanichaya *et al.* 2018; Ge *et al.* 2022).

By varying the light intensity, the photocatalytic performance of the TiO_2@UiO-66 composite under different irradiation conditions was evaluated. As shown in Figure 8(b), when the light intensity increased to 20 mW cm^{-2}, the microplastic removal efficiency reached 78.3%, whereas under weak illumination (4 mW cm^{-2}) the efficiency was only 63.4% after 30 h of UV irradiation. In general, higher light intensity provides a greater flux of incident photons per unit volume, thereby generating more reactive species on the catalyst surface and consequently enhancing the reaction rate. However, the removal efficiency decreases significantly – and is nearly negligible – when control experiments are conducted in the absence of light (Allé *et al.* 2021; García-Muñoz *et al.* 2022).

The surface morphology of the TiO_2@UiO-66 catalyst after the photocatalytic degradation of PSMPs is shown in Figure 9(a) and 9(b). It can be observed that several PS fibers remain adhered to the catalyst surface after 30 h of reaction, while the rest of the catalyst surface appears relatively smooth and retains a morphology similar to that of pristine TiO_2@UiO-66 before the reaction. This indicates that the majority of PSMPs were degraded by the photocatalyst during UV irradiation, and the degradation process would continue upon prolonging the irradiation time. Figure 9(c) presents

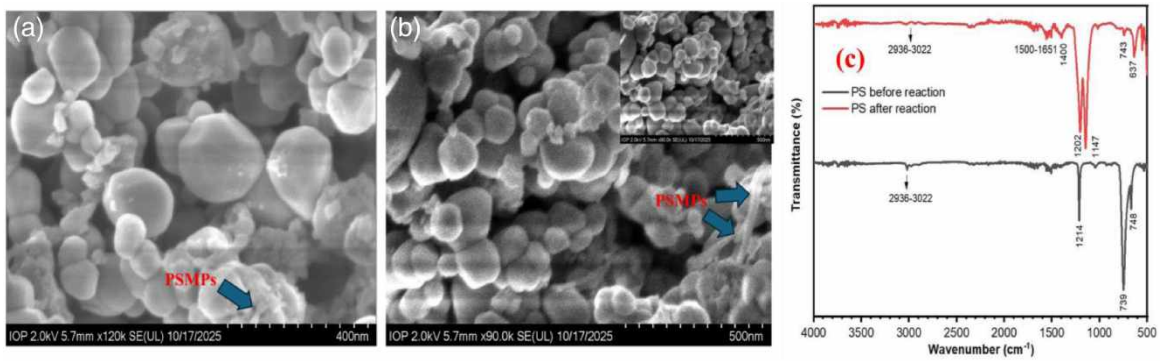

Figure 9 | SEM images of the TiO_2@UiO-66 catalyst after the photocatalytic degradation of polystyrene microplastics (inset: pristine TiO_2-@UiO-66 before reaction) (a,b), and FT-IR spectra of PS microplastics before and after photocatalytic oxidation (c).

the FT-IR spectra of PS microplastics before and after photocatalytic oxidation. The characteristic absorption bands of pristine PS were observed at 748 cm^{-1}, corresponding to the out-of-plane C–H bending vibration of the aromatic ring (Kumar *et al.* 2015); 1214 cm^{-1}, associated with the C–H deformation vibration; 2,936 cm^{-1}, assigned to the alkyl (–CH_2–) stretching vibrations from the polymer backbone (Mylläri *et al.* 2015), and 3,022 cm^{-1}, attributed to the = C–H stretching of the aromatic ring (Chen *et al.* 2001).

After photocatalytic oxidation, new absorption bands appeared at 1,147 cm^{-1}, corresponding to the C–O stretching vibration of aryl–alkyl ether groups, and at 637 cm^{-1}, assigned to the out-of-plane ring deformation of carbonyl (–C = O) groups adjacent to aromatic rings (Zan *et al.* 2006). These results suggest the formation of new oxygen-containing functional groups, including aryl ether (–O–R) and carbonyl (–C = O) moieties, as a result of the oxidative degradation of PSMPs. The emergence of these oxygenated groups confirms that photocatalytic oxidation over TiO_2@UiO-66 effectively breaks the polymer chains and introduces oxygen functionalities onto the PS structure, indicating the progression of PS mineralization.

3.3. Identification of reactive oxygen species and photodegradation mechanism of PSMPs

To elucidate the photocatalytic mechanism responsible for the degradation of polystyrene microplastics, radical trapping experiments were carried out to identify the dominant reactive oxygen species (ROS) involved in the TiO_2@UiO-66-catalyzed process. The generation of ROS is generally regarded as the key factor determining the efficiency of photocatalytic degradation in aqueous systems. The experiments were performed under controlled conditions (PSMPs concentration of 150 ppm, fixed temperature and pH) using TiO_2@UiO-66 as the photocatalyst. Specific scavengers were introduced to capture different reactive species: tert-butyl alcohol (TBA) for hydroxyl radicals ($^{\cdot}OH$), *p*-benzoquinone (BQ) for superoxide radicals ($O_2^{\cdot-}$), and formic acid (FA) for photogenerated holes (h^+).

As shown in Figure 10, the degradation efficiency of PSMPs reached 63% in the absence of scavengers after 30 h of UV irradiation. The addition of TBA and BQ significantly suppressed the degradation efficiency to 17.3 and 43.5%, respectively, indicating that $^{\cdot}OH$ and $O_2^{\cdot-}$ radicals play a predominant role in the photocatalytic process. In contrast, the addition of FA only slightly affected the degradation efficiency (61.2%), suggesting a minor contribution from photogenerated holes. These findings confirm that $^{\cdot}OH$ and $O_2^{\cdot-}$ are the major reactive species responsible for the photodegradation of PSMPs using TiO_2@UiO-66. The results are consistent with the observations of He *et al.* (2023), who reported that $^{\cdot}OH$ and $O_2^{\cdot-}$ were the dominant ROS in the photocatalytic degradation of polystyrene microplastics coupled with hydrogen evolution over an FeB/TiO_2 composite. Similarly, Rodríguez-Olivares *et al.* (2025) demonstrated that $^{\cdot}OH$ and $O_2^{\cdot-}$ were the key oxidative species driving the degradation of nylon-6 using an HKUST-1(Cu/Fe)-derived CuO/TiO_2 photocatalyst. The formation of hydroxyl radicals ($^{\cdot}OH$) can occur either through the oxidation of water molecules by photogenerated holes or via a series of redox reactions involving photogenerated electrons and superoxide radicals ($O_2^{\cdot-}$) (Xu *et al.* 2021). Typically,

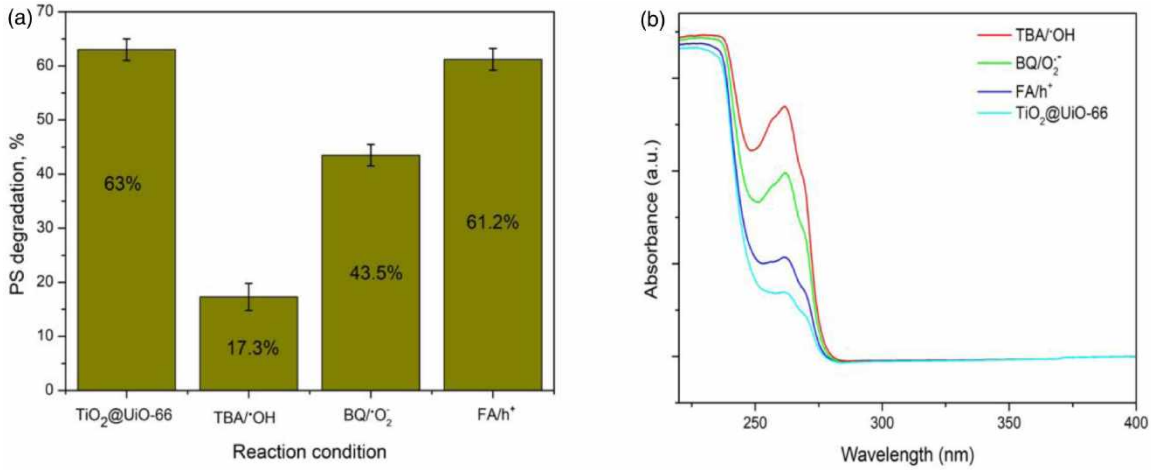

Figure 10 | Identification of reactive oxygen species: Photocatalytic degradation efficiency of PSMPs under different radical-scavenging conditions (a), UV–Vis absorption spectra of TiO_2@UiO-66 in the presence of various scavengers – TBA for $^{\bullet}OH$, BQ for $O_2^{\cdot-}$, and FA for h^+ (b). (Conditions: 1.0 g/L of photocatalyst; scavenger = 3.5 mM; PSMPs = 150 ppm; natural pH, room temperature, light intensity = 4 mW·cm^{-2}).

this process begins with the reduction of molecular oxygen by excited electrons to generate $O_2^{\cdot-}$, which subsequently reacts with protons (h^+) to produce hydroperoxyl radicals ($HO^{\cdot}$). Subsequent transformations of $HO^{\cdot}$ and $O_2^{\cdot-}$ species yield highly reactive $^{\cdot}OH$ radicals (Parrino *et al.* 2020; Hussain *et al.* 2022).

Based on the UV–Vis diffuse reflectance spectroscopy results, the main charge transfer pathway in the TiO_2@UiO-66 semiconductor composite under visible-light irradiation is illustrated in Figure 11. The proposed mechanism was established by determining the valence band (VB) and conduction band (CB) edge potentials of TiO_2 and UiO-66 from their band gap energies using the Mulliken electronegativity approach.

The band edge positions were calculated according to the following equations:

$$E_{CB} = \chi - E_e - 0.5E_g$$
$$E_{VB} = E_g + E_{CB}$$

where χ is the absolute electronegativity of the semiconductor (eV), $E_e = 4.5$ eV represents the energy of free electrons on the vacuum scale, and E_g is the band gap energy (eV).

Using the reported absolute electronegativity values of UiO-66 (χ = 5.4 eV) (Federica *et al.* 2021) and TiO_2 (χ = 5.81 eV) (Girish *et al.* 2022; Nada *et al.* 2025), together with their corresponding band gap energies of 3.06 and 3.27 eV, respectively, the CB and VB positions were calculated. The estimated CB and VB potentials of UiO-66 are −0.63 and +2.43 eV (vs. NHE), whereas those of TiO_2 are −0.33 and +2.94 eV. The relative band alignment indicates that the CB level of UiO-66 is more negative than that of TiO_2, while the VB level of TiO_2 is more positive than that of UiO-66, suggesting favorable charge separation within the composite system.

The TiO_2@UiO-66 system forms an S-scheme heterojunction, in which selective recombination occurs between the electrons in the CB of TiO_2 (due to its higher CB energy level) and the holes in the VB of UiO-66 (owing to its lower VB energy level). This recombination pathway preserves the electrons with strong reduction potential in the CB of UiO-66, which effectively reduce O_2 to generate $\cdot O_2^-$ radicals, as well as the holes with strong oxidation potential in the VB of TiO_2, which facilitate the formation of $^{\cdot}OH$ radicals. As a result, the catalyst exhibits enhanced charge separation efficiency while simultaneously optimizing its redox capability, leading to superior photocatalytic performance.

The intermediate products generated during the photodegradation of polystyrene microplastics were analyzed by LC/MS (Figure S2 and Figure 12). Hydroperoxyl ($HO^{\cdot}$) and superoxide ($O_2^{\cdot-}$) radicals attack the unstable sites of the PS chains, initiating a series of bond-cleavage reactions that break the polymer into smaller molecular fragments, eventually yielding CO_2 and H_2O (Uheida *et al.* 2021). Specifically, these reactive oxygen species preferentially target the tertiary carbon sites, leading to C–C bond scission and the formation of $C_{23}H_{22}O$ (*m/z* 314.61). This intermediate undergoes further oxidative chain scission to generate $C_{16}H_{18}O_4$ (*m/z* 273.77), $C_{16}H_{14}O_2$ (*m/z* 238.87), and $[C_{15}H_{14}O + H]^+$ (*m/z* 213.93). These products

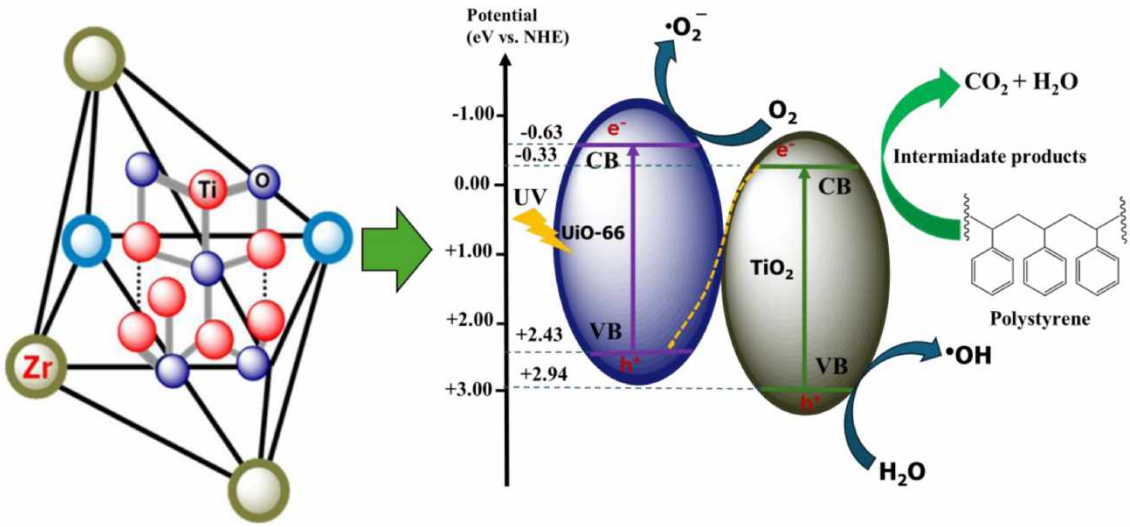

Figure 11 | The proposed mechanisms for the electron transfers under UV irradiation.

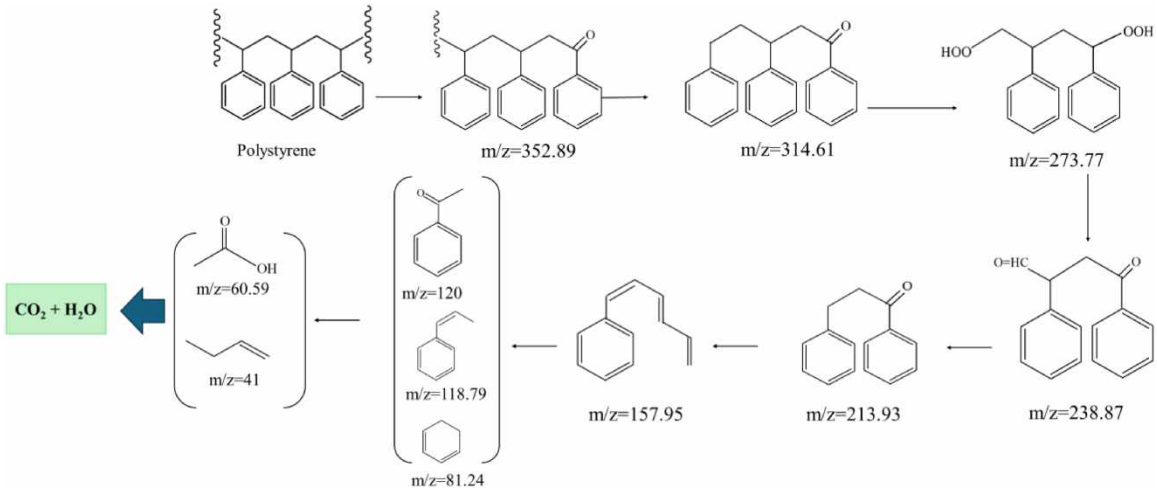

Figure 12 | Proposed photocatalytic degradation mechanism of polystyrene microplastics over TiO_2@UiO-66 composite.

subsequently react with radical species through ring-opening and oxidation pathways, producing shorter-chain compounds such as phenylacetaldehyde (C_8H_8O, *m/z* 120), C_9H_{10} (*m/z* 118.79), cyclohexadiene (*m/z* 81.24), acetic acid (m/z 60), and the allyl cation (*m/z* 41.56). Ultimately, continuous oxidation converts these intermediates into the inorganic end products CO_2 and H_2O.

The degradation efficiency of PS microplastics over the TiO_2@UiO-66 catalyst, compared with several other advanced oxidation technologies, is presented in Table 1.

Conventional TiO_2-based photocatalysts generally show limited mineralization of PS microplastics, achieving only 20–40% degradation and <30% TOC removal after prolonged UV irradiation, indicating predominant surface oxidation rather than complete chain scission. ZnO under visible light performs similarly due to rapid charge recombination. Although photo-Fenton and ozonation enhance degradation (40–60%) and mineralization (30–50%), they rely on homogeneous oxidants, reducing sustainability.

In contrast, TiO_2@UiO-66 achieved 63% degradation and 56.8% TOC removal within 30 h, outperforming most heterogeneous TiO_2 systems and rivaling advanced oxidation processes without external oxidants. The superior performance is

Table 1 | Comparison of photocatalytic degradation of PS microplastics

Catalyst/reaction system	Light source	Reaction time	Degradation efficiency	TOC mineralization	Reference
Photo-Fenton system	UV + H_2O_2	6–24 h	40–60%	Higher mineralization (≈30–50%)	Di Luca *et al.* (2023)
Ozonation	O_3	2–6 h	30–50%	Moderate mineralization	Gayathri *et al.* (2023)
ZnO	Visible light	24 h	20–35%	10–25% TOC removal	Uheida *et al.* (2021)
Bio-derived porous N–TiO_2	UV	12–48 h	~30–40% (significant increase in carbonyl index)	Low mineralization (<20% TOC removal)	Ariza-Tarazona *et al.* (2019)
TiO_2-based systems	UV irradiation	24–48 h	~20–40%	10–30% TOC removal	Zan *et al.* (2004)
Ag-TiO_2/CNT hybrid nanocomposite	Solar irradiation	48 h	~31.7%	–	Chinnam *et al.* (2024)
TiO_2@UiO-66	UV irradiation	30 h	63%	56.8% TOC removal at PS concentration of 200 ppm	This study

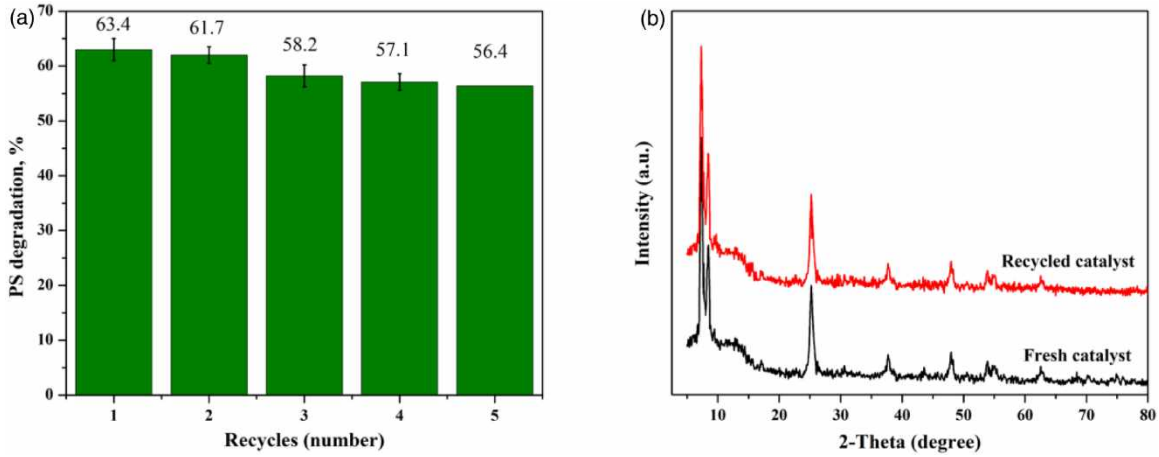

Figure 13 | (a) Reusability of the TiO_2@UiO-66 photocatalyst for PS degradation, and (b) XRD patterns of the fresh and recycled catalysts. (Conditions: 1.0 g/L of catalyst; natural pH, room temperature, light intensity = 4 mW·cm^{-2}).

attributed to improved charge separation at the TiO_2–MOF interface and the confinement-enhanced adsorption of PS, promoting efficient ROS-mediated C–C bond cleavage and deeper mineralization. These results highlight heterojunction engineering with porous frameworks as a promising strategy for sustainable microplastic remediation.

3.3. Evaluation of catalytic stability

After the photocatalytic degradation of PS microplastics, the powdered catalyst was primarily recovered by centrifugation at 5,000 rpm for 10 min to ensure complete separation of the solid phase from the reaction solution. The collected solid was washed several times with distilled water to remove soluble mineralization products, followed by additional washing with ethanol to eliminate residual organic intermediates adsorbed on the catalyst surface. The sample was then dried at 80 °C for 12 h to remove moisture. After treatment, the catalyst was stored in a sealed container prior to reuse in subsequent cycles. The PS degradation efficiency on TiO_2@UiO-66 catalyst after 5 reaction cycles is shown in Figure 13(a).

The recyclability test demonstrates that the catalyst maintains high photocatalytic stability over repeated cycles. The PS degradation efficiency decreases only slightly from 63.4% in the first run to 56.4% after five cycles, corresponding to a minor activity loss of approximately 7% in absolute terms. The absence of abrupt deactivation indicates that most active sites remain accessible, and no significant photocorrosion or metal leaching occurs during the reaction. The slight decline in activity is more likely associated with surface fouling by intermediate oxidation products or minor catalyst loss during recovery rather than intrinsic structural degradation.

This stability is further confirmed by the XRD patterns (Figure 13(b)), where the recycled catalyst exhibits nearly identical diffraction peak positions compared to the fresh sample. No new crystalline phases or peak shifts are observed, indicating that the crystal structure remains intact after repeated photocatalytic operation. Although a slight reduction in peak intensity is visible, this can be attributed to surface adsorption of residual species rather than framework collapse or phase transformation. The combined catalytic performance and structural analyses therefore confirm that the catalyst possesses robust structural integrity and good reusability, making it a promising candidate for sustainable microplastic remediation.

3. CONCLUSIONS

The UiO-66 combined with TiO_2 semiconductor was successfully synthesized through a simple solvent method followed by thermal treatment. The obtained TiO_2@UiO-66 composite exhibited superior photocatalytic performance compared to pristine TiO_2 and UiO-66 in the degradation of polystyrene microplastics. The TiO_2@UiO-66 catalyst displayed the anatase crystalline phase of TiO_2 and demonstrated excellent photocatalytic activity under UV irradiation for polystyrene degradation at ambient pH conditions. This was evidenced by the decrease in TOC concentration from 138 mg/L (corresponding to 150 ppm PSMPs) to 51.23 mg/L after 30 h of irradiation. SEM images, FT-IR, and LC/MS analyses confirmed the oxidation and scission of polymer chains during photocatalytic degradation, resulting from the synergistic interaction between UiO-66 and TiO_2. This process led to the formation of intermediate and low-molecular-weight products

such as aldehydes and carboxylic acids. The enhanced photocatalytic efficiency is attributed to the interfacial coupling effect between TiO_2 and UiO-66, which promotes efficient separation and transfer of photogenerated electron–hole pairs.

ACKNOWLEDGEMENTS

The authors gratefully acknowledge the financial support provided by the Ministry of Education and Training of Vietnam through the research project coded B2024-MDA-10.

CREDIT AUTHORSHIP CONTRIBUTION STATEMENT

Xuan Nui Pham: Methods, Formal analysis, Project administration, Funding acquisition, Review and editing of the manuscript. **Huan V. Doan:** Investigation, Methods, Validation, Formal analysis, Data curation. **T.-Thanh-Bao Nguyen:** Validation, Review and editing of the manuscript, Solfwave, Study supervision.

DATA AVAILABILITY STATEMENT

All relevant data are included in the paper or its Supplementary Information.

CONFLICT OF INTEREST

The authors declare there is no conflict.

REFERENCES

Alisha, K., Marie, L. P., Alireza, R., Diana, D., Bahena-Uribe, D., Colbeau-Justin, C., Herrero, C., Rutkowska-Zbik, D., Deschamps, J. & Remita, H. (2025) Cu-Based MOF/TiO_2 composite nanomaterials for photocatalytic hydrogen generation and the role of copper, *Advanced Functional Materials*, **2025**, 2501736. doi:10.1002/adfm.202501736.

Allé, P. H., Garcia-Muñoz, P., Adouby, K., Keller, N. & Robert, D. (2021) Efficient photocatalytic mineralization of polymethylmethacrylate and polystyrene nanoplastics by TiO_2/β-SiC alveolar foams, *Environmental Chemistry Letters*, **19**, 1803–1808. doi:10.1007/s10311-020-01099-2.

Amjad, M., Intisar, A., Afzal, A. & Hussain, N. (2023) Biological methods for the removal of microplastics from water, *Advances in Chemical Pollution, Environmental Management and Protection*, **9**, 65–78. doi:10.1016/bs.apmp.2022.10.003.

Ariza-Tarazona, M. C., Villarreal-Chiu, J. F., Barbieri, V., Siligardi, C. & Cedillo-Gonzalez, E. I. (2019) New strategy for microplastic degradation: green photocatalysis using a protein-based porous N–TiO_2 semiconductor, *Ceramics International*, **45** (7), 9618–9624. doi:10.1016/j.ceramint.2018.10.208.

Ariza-Tarazona, M. C., Villarreal-Chiu, J. F., Hernández-López, J. M., Rivera de la Rosa, J., Barbieri, V., Siligardi, C. & Cedillo-González, E. I. (2020) Microplastic pollution reduction by a carbon and nitrogen-doped TiO_2: effect of pH and temperature in the photocatalytic degradation process, *Journal of Hazardous Materials*, **395**, 122632. doi:10.1016/j.jhazmat.2020.122632.

Bora, L. & Mewada, R. (2017) Visible/solar light active photocatalysts for organic effluent treatment: fundamentals, mechanisms and parametric review, *Renewable and Sustainable Energy Reviews*, **76**, 1393–1421.

Cao, W., Ren, H., Cai, C., Li, D., Li, T., Lou, C. & Lin, J. (2023) Preparation of UiO-66-NH_2/$Bi_{2.15}WO_6$ composite with enhanced tetracycline degradation under weak light intensity, *Research on Chemical Intermediates*, **49** (10), 4257–4274. doi:10.1007/s11164-023-05080-w.

Chen, G., Liu, S., Chen, S. & Qi, Z. (2001) FTIR spectra, thermal properties, and dispersibility of a polystyrene/montmorillonite nanocomposite, *Macromolecular Chemistry Physics*, **202**, 1189–1193.

Chen, H. W., Ku, Y. & Kuo, Y. L. (2007) Photodegradation of o-cresol with Ag-deposited TiO_2 under visible and UV light irradiation, *Chemical Engineering Technology*, **30**, 1242–1247. doi:10.1002/ceat.200700196.

Chinnam, B., Dasagiri, C. S. & Araga, R. (2024) Synthesis and preliminary evaluation of Ag-TiO_2/CNT hybrid nanocomposite for the degradation of polystyrene microplastics under solar irradiation, *Environmental Science and Pollution Research*, **31**, 32863–32874. doi:10.1007/s11356-024-33438-z.

Danilo, B. S. & Ana, C. M. (2025) TiO_2-based photocatalytic degradation of microplastics in water: current status, challenges and future perspectives, *Journal of Water Process Engineering*, **72**, 107465. doi:10.1016/j.jwpe.2025.107465.

Di Luca, C., Garcia, J., Ortiz, D., Munoz, M., Carbajo, J., de Pedro, Z. M. & Casas, J. A. (2023) Mineralization of polystyrene nanoplastics in water by photo-Fenton oxidation, *Journal of Environmental Chemical Engineering*, **11**, 110755. doi:10.1016/j.jece.2023.110755.

Doan, H. V., Nguyen, H. T., Ting, V. P., Guan, S., Eloi, J.-C., Hall, S. R. & Pham, X. N. (2021) Improved photodegradation of anionic dyes using a complex graphitic carbon nitride and iron-based metal–organic framework material, *Faraday Discussions*, **231**, 81–96. doi:10.1039/D1FD00010A.

Domínguez-Jaimes, L. P., Cedillo-González, E. I., Luévano-Hipólito, E., Acuña-Bedoya, J. D. & Hernández-López, J. M. (2021) Degradation of primary nanoplastics by photocatalysis using different anodized TiO_2 structures, *Journal of Hazardous Materials*, **413**, 125452. doi:10.1016/j.jhazmat.2021.125452.

Fa, W., Guo, L., Wang, J., Guo, R., Zheng, Z. & Yang, F. (2012) Solid-phase photocatalytic degradation of polystyrene with $TiO_2/Fe(St)_3$ as catalyst, *Journal of Applied Polymer Science*, **125**, 37751. doi:10.1002/app.37751.

Federica, Z., Lawson, T. G., Sanggyu, C., Siyu, C., Jihan, K., David, F.-J., Bartomeu, M. & Peyman, Z. M. (2021) Computational techniques for characterisation of electrically conductive MOFs: quantum calculations and machine learning approaches, *Journal of Materials Chemistry C*, **9**, 13584–13599. doi:10.1039/D1TC02543K.

Galgani, F., Hanke, G., Werner, S. & De Vrees, L. (2013) Marine litter within the European marine strategy framework directive, *ICES Journal of Marine Science*, **70**, 1055–1064.

García-Muñoz, P., Allé, P. H., Bertoloni, C., Torres, A., Ulagares de la Orden, M., Urreaga, J. M., Dziurla, M.-A., Fresno, F., Robert, D. & Keller, N. (2022) Photocatalytic degradation of polystyrene nanoplastics in water. A methodological study, *Journal of Environmental Chemical Engineering*, **10**, 108195. doi:10.1016/j.jece.2022.108195.

Gayathri, P. V., Joseph, S., Mohan, M. & Pillai, D. (2023) Advanced oxidation processes for the degradation of microplastics from the environment: a review, *Water and Environment Journal*, **37**, 686–701. doi:10.1111/wej.12883.

Ge, J., Zhang, Z., Ouyang, Z., Shang, M., Liu, P., Li, H. & Guo, X. (2022) Photocatalytic degradation of (micro)plastics using TiO_2-based and other catalysts: properties, influencing factor, and mechanism, *Environmental Research*, **209**, 112729. doi:10.1016/j.envres.2022.112729.

Girish, Y. R., Udayabhanu, C. G., Gubran, A., Abdo, H., Mysore, B. N., Ganganagappa, N. & Kullaiah, B. (2022) Facile and rapid synthesis of solar-driven $TiO_2/g\text{-}C_3N_4$ heterostructure photocatalysts for enhanced photocatalytic activity, *Journal of Science: Advanced Materials and Devices*, **7**, 100419. doi:10.1016/j.jsamd.2022.100419.

González-Pleiter, M., Tamayo-Belda, M., Pulido-Reyes, G., Amariei, G., Leganés, F., Rosal, R. & Fernández-Piñas, F. (2019) Secondary nanoplastics released from a biodegradable microplastic severely impact freshwater environments, *Environmental Science: Nano*, **6**, 1382–1392. doi:10.1039/C8EN01427B.

He, J., Han, L., Ma, W., Chen, L., Ma, C., Xu, C. & Yang, Z. (2023) Efficient photodegradation of polystyrene microplastics integrated with hydrogen evolution: uncovering degradation pathways, *iScience*, **26** (6), 106833. doi:10.1016/j.isci.2023.106833.

Hussain, T., Hussain, M., Hussain, S. & Kaseem, M. (2022) Microwave-assisted synthesis of $nite_2$ photocatalyst as a facile and scalable approach for energy-efficient photocatalysis and detoxification of harmful organic dyes, *Separation and Purification Technology*, **282**, 120025. doi:10.1016/j.seppur.2021.120025.

Jeyaraj, J. & Baskaralingam, V. (2023) Combined toxic effect of environmental predominant microplastics and ZnO nanoparticles in freshwater snail *Pomaceae paludosa*, *Environmental Pollution*, **325**, 121427. doi:10.1016/j.envpol.2023.121427.

Jianhua, G., Zhiping, Z., Zhuozhi, O., Mengxin, S., Peng, L., Huang, L. & Xuetao, G. (2022) Photocatalytic degradation of (micro)plastics using TiO 2-based and other catalysts: properties, influencing factor, and mechanism, *Environmental Research*, **209**, 112729. doi:10.1016/j.envres.2022.112729.

Karimi Estahbanati, M. R., Kiendrebeogo, M., Mostafazadeh, A. K., Drogui, P. & Tyagi, R. D. (2021) Treatment processes for microplastics and nanoplastics in waters: state-of-the-art review, *Marine Pollution Bulletin*, **168**, 112374. doi:10.1016/j.marpolbul.2021.112374.

Kögel, T., Bjorøy, Ø., Toto, B., Bienfait, A. M. & Sanden, M. (2020) Micro- and nanoplastic toxicity on aquatic life: determining factors, *Science of the Total Environment*, **709**, 136050. doi:10.1016/j.scitotenv.2019.136050.

Kumar, A., Jangir, L. K., Kumari, Y., Kumar, M., Kumar, V. & Awasthi, K. (2015) Optical and structural study of polyaniline/polystyrene composite films, *Macromolecular Symposia*, **357**, 229–234. doi:10.1002/MASY.201500039.

Law, K. L. (2017) Plastics in the marine environment, *Annual Review of Marine Science*, **9**, 205–229.

Li, S., Peng, W., Guo, Y., Li, S. & Wang, Q. (2024) Current status of microplastic pollution and the latest treatment technologies, *Science of The Total Environment*, **957**, 177467. doi:10.1016/j.scitotenv.2024.177467.

Lim, T. T., Yap, P. S., Srinivasan, M. & Fane, A. G. (2011) Tio_2/AC composites for synergistic adsorption–photocatalysis processes: present challenges and further developments for water treatment, *Critical Reviews in Environmental Science and Technology*, **41** (13), 1173–1230. doi:10.1080/10643380903488664.

Montenegro, R., González, Z., Rodríguez, A., Canovi, C., Pozzi, P., Siligardi, C. & Cedillo-González, E. I. (2025) Processing of bio-based photocatalytic sponge-like structures containing C,N–TiO_2 colloidally dispersed onto cellulose nanofibers for microplastic remediation, *Journal of Environmental Management*, **389**, 126015.

Mylläri, V., Ruoko, T. P. & Syrjälä, S. (2015) A comparison of rheology and FTIR in the study of polypropylene and polystyrene photodegradation, *Journal of Applied Polymer Science*, **132**, 42246. doi:10.1002/app.42246.

Nada, D. A., Razan, M. S., Ibtisam, M., Reem, G., Omaymah, A., Saham, F. I., Kamelah, S. A. & Fathy, S. (2025) Synthesis and investigation of TiO_2/Na-mordenite nanocomposite for photocatalytic degradation of acid red 57 dye: experimental design optimization, *Arabian Journal of Chemistry*, **18**, 1282025. doi:10.25259/AJC_128_2025.

Nguyen, H. V. T., Nguyen, M. B., Doan, H. V. & Pham, X. N. (2023) A green synthesis of $cuins_2$/MIL-101(Cr) nanocomposite with efficient visible-light-induced photocatalytic activity, *Materials Research Express*, **10**, 085506. Doi:10.1088/2053-1591/acf18f.

Padervand, M., Lichtfouse, E., Robert, D. & Wang, C. (2020) Removal of microplastics from the environment: a review, *Environmental Chemistry Letters*, **18** (8), 807–828. doi:10.1007/s10311-020-00983-1.

Parrino, F., Livraghi, S., Giamello, E., Ceccato, R. & Palmisano, L. (2020) Role of hydroxyl, superoxide, and nitrate radicals on the fate of bromide ions in photocatalytic TiO_2 suspensions, *ACS Catalysis*, **10** (14), 7922–7931.

Petri, M. L., Ekta, R., Assa Aravindh, S. D., Harishchandra, S., Graham, K., Matti, A., Wei, C. & Marko, H. (2020) Synergistic effect of Ni–Ag–rutile TiO_2 ternary nanocomposite for efficient visible-light-driven photocatalytic activity, *RSC Advances*, **10**, 36930–36940. doi:10.1039/D0RA07078E.

Pham, X. N., Vu, V.-T., Nguyen, H. V. T., Nguyen, T.-T.-B. & Doan, H. V. (2022) Designing a novel heterostructure agins$_2$@MIL-101(Cr) photocatalyst from PET plastic waste for tetracycline degradation, *Nanoscale Advances*, **4**, 3600–3608. doi:10.1039/D2NA00371F.

Qahtan, T. F., Owolabi, T. O. & Saleh, T. A. (2024) X-ray photoelectron spectroscopy of surface-treated TiO_2 mesoporous film by 500 eV argon ion beam, *Journal of Molecular Liquids*, **393**, 123556. doi:10.1016/j.molliq.2023.123556.

Raji, R. & Gopchandran, K. G. (2019) Plasmonic photocatalytic activity of ZnO:Au nanostructures: tailoring the plasmon absorption and interfacial charge transfer mechanism, *Journal of Hazardous Materials*, **368**, 345–357. doi:10.1016/j.jhazmat.2019.01.052.

Ramasubbu, V., Kumar, P. R., Chellapandi, T., Madhumitha, G., Mothi, E. M. & Shajan, X. S. (2022) Zn(II) porphyrin-sensitized (TiO_2@Cd-MOF) nanocomposite aerogel as novel photocatalyst for effective degradation of methyl orange dye, *Optical Materials*, **132**, 112558. doi:10.1016/j.optmat.2022.112558.

Rodríguez-Olivares, Á. E., Guzmán-Mar, J. L., Quero-Jiménez, P. C., Montemayor, S. M., Maya-Treviño, L. & Hinojosa-Reyes, L. (2025) Analytical approaches to track nylon 6 microplastic fiber degradation using HKUST-1(Cu/Fe)-derived CuO/TiO_2 photocatalyst, *Journal of Water Process Engineering*, **71**, 107192. doi:10.1016/j.jwpe.2025.107192.

Rojas-Guerrero, C. A., Villanueva-Rodríguez, M., Guzmán-Mar, J. L., Hernández-Ramírez, A., Cedillo-González, E. I., Longoria Rodríguez, F. E. & Hinojosa-Reyes, L. (2023) Solar photocatalytic degradation of polyethylene terephthalate nanoplastics using TiO_2/MIL-100(Fe) composite, *Journal of Environmental Chemical Engineering*, **11**, 110415. doi:10.1016/j.jece.2023.110415.

Schirinzi, G. F., Pérez-Pomeda, I., Sanchís, J., Rossini, C., Farré, M. & Barceló, D. (2017) Cytotoxic effects of commonly used nanomaterials and microplastics on cerebral and epithelial human cells, *Environmental Research*, **159**, 579–587.

Shang, J., Chai, M. & Zhu, Y. (2003) Solid-phase photocatalytic degradation of polystyrene plastic with TiO_2 as photocatalyst, *Journal of Solid State Chemistry*, **174** (1), 104–110. doi:10.1016/S0022-4596(03)00183-X.

Talal, F. Q., Taoreed, O. O. & Tawfik, A. S. (2024) X-ray photoelectron spectroscopy of surface-treated TiO_2 mesoporous film by 500 eV argon ion beam, *Journal of Molecular Liquids*, **393**, 123556. doi:10.1016/j.molliq.2023.123556.

Tofa, T. S., Kunjali, K. L., Paul, S. & Dutta, J. (2019a) Visible light photocatalytic degradation of microplastic residues with zinc oxide nanorods, *Environmental Chemistry Letters*, **17**, 1341–1346. doi:10.1007/s10311-019-00859-z.

Tofa, T. S., Ye, F., Kunjali, K. L. & Dutta, J. (2019b) Enhanced visible light photodegradation of microplastic fragments with plasmonic platinum/zinc oxide nanorod photocatalysts, *Catalysts*, **9** (10), 819. doi:10.3390/catal9100819.

Uheida, A., Dutta, J., Giraldo Mejía, H., Abdel-Rehim, M. & Hamd, W. (2021) Visible light photocatalytic degradation of polypropylene microplastics in a continuous water flow system, *Journal of Hazardous Materials*, **406**, 124299. doi:10.1016/j.jhazmat.2020.124299.

Valenzano, L., Civalleri, B., Chavan, S., Bordiga, S., Nilsen, M. H., Jakobsen, S., Lillerud, K. P. & Lamberti, C. (2011) Disclosing the complex structure of UiO-66 metal–organic framework: a synergic combination of experiment and theory, *Chemistry of Materials*, **23**, 1700–1718.

Viana, A. M., Ribeiro, S. O., de Castro, B., Balula, S. S. & Cunha-Silva, L. (2019) Influence of UiO-66(Zr) preparation strategies on its catalytic efficiency for desulfurization process, *Materials*, **12** (18), 3009. doi:10.3390/ma12183009.

Wanichaya, M., Titarat, T., Wisanu, P. & Keiichi, I. (2018) Photocatalytic properties and plastic degradation of TiO_2 nanocomposite with synthetic – rutile from natural ore, *Journal of the Japan Society of Powder and Powder Metallurgy*, **65** (11), 719–724. doi:10.2497/jjspm.65.719.10.2497/jjspm.65.719.

Xu, X., Wang, J., Chen, T., Yang, N., Wang, S., Ding, X. & Chen, H. (2021) Deep insight into ROS-mediated direct and hydroxylated dichlorination process for efficient photocatalytic sodium pentachlorophenate mineralization, *Applied Catalysis B: Environmental*, **296**, 120352. doi:10.1016/j.apcatb.2021.120352.

Xueqin, W., Siow, H. T., Mohd, R. S. & Newati, W. (2025) Photocatalytic degradation of organic pollutants and microplastics using Ag/TiO_2: recent advances in mechanism, synthesis and propertie, *Water Air Soil Pollution*, **236** (30), 1–25. doi:10.1007/s11270-024-07669-2.

Zan, L., Tian, L., Liu, Z. & Peng, Z. (2004) A new polystyrene–TiO_2 nanocomposite film and its photocatalytic degradation, *Applied Catalysis A: General*, **264**, 237–242. doi:10.1016/j.apcata.2003.12.046.

Zan, L., Wang, S., Fa, W., Hu, Y., Tian, L. & Deng, K. (2006) Solid-phase photocatalytic degradation of polystyrene with modified nano-TiO_2 catalyst, *Polymer*, **47** (24), 8155–8162. doi:10.1016/j.polymer.2006.09.023.

First received 30 November 2025; accepted in revised form 8 April 2026. Available online 26 May 2026